New Phytologist

Research

Mp*TCP1* controls cell proliferation and redox processes in *Marchantia polymorpha*

Andrea Busch[1]*, Marek Deckena[1]*, Marilia Almeida-Trapp[2], Sarah Kopischke[1], Cilian Kock[1], Esther Schüssler[1], Miltos Tsiantis[3], Axel Mithöfer[2] and Sabine Zachgo[1]

[1]Botany, University of Osnabrück, Osnabrück 49076, Germany; [2]Max Planck Institute for Chemical Ecology, Jena 07745, Germany; [3]Max Planck Institute for Plant Breeding Research, Cologne 50829, Germany

Author for correspondence:
Sabine Zachgo
Tel: +49 541 9692840
Email: zachgo@biologie.uni-osnabrueck.de

Received: *21 May 2019*
Accepted: *26 July 2019*

New Phytologist (2019) **224:** 1627–1641
doi: 10.1111/nph.16132

Key words: cell proliferation, DNA binding, evolution, *Marchantia polymorpha*, redox regulation, secondary metabolites, TCP.

Summary

- TCP transcription factors are key regulators of angiosperm cell proliferation processes. It is unknown whether their regulatory growth capacities are conserved across land plants, which we examined in liverworts, one of the earliest diverging land plant lineages.
- We generated knockout mutants for Mp*TCP1*, the single TCP-P clade gene in *Marchantia polymorpha*, and characterized its function by conducting cell proliferation and morphological analyses as well as messenger RNA expression, transcriptome, chemical, and DNA binding studies.
- Mp*tcp1*^{ge} lines show a reduced vegetative thallus growth and extra tissue formation in female reproductive structures. Additionally, mutant plants reveal increased hydrogen peroxide (H_2O_2) levels and an enhanced pigmentation in the thallus caused by formation of secondary metabolites, such as aminochromes. MpTCP1 proteins interact redox dependently with DNA and regulate the expression of a comprehensive redox network, comprising enzymes involved in H_2O_2 metabolism.
- Mp*TCP1* regulates Marchantia growth in a context-dependent manner. Redox sensitivity of the DNA binding capacity of MpTCP1 proteins provides a mechanism to respond to altered redox conditions. Our data suggest that Mp*TCP1* activity could thereby have contributed to diversification of land plant morphologies and to adaptations to abiotic and biotic challenges, as experienced by liverworts during early land plant colonization.

Introduction

In multicellular plant development, final organ size and whole plant body architecture are controlled by the spatiotemporal regulation of cell proliferation and cell differentiation processes, integrating the response to environmental stimuli. Angiosperm stem cell pools reside in meristematic regions of the shoot and root and maintain indeterminate growth throughout plant life. The meristematic cell division zone is surrounded by a differentiation region where cell proliferation is terminated through cell expansion. Determinate and indeterminate growth together govern plant morphogenesis, requiring a tight linkage and coordination.

The plant-specific TCP transcription factors (TFs) exert crucial regulatory functions in diverse developmental processes. Based on sequence similarity of the DNA-binding TCP domain, TCP genes group into the TCP-P (class I) and TCP-C (class II) clades (Martin-Trillo & Cubas, 2010). Analysis of TCP genes, particularly *TEOSINTE BRANCHED1* (*TB1*) and *CYCLOIDEA* (*CYC*), revealed a contribution to the evolution of novel plant morphologies. *TB1* from the TCP-C clade is a key regulator for apical dominance during the domestication of maize (*Zea mays*) by repressing the outgrowth of axillary meristems (Doebley *et al.*, 1997). The TCP-C gene *CYC* from *Antirrhinum* mediates floral zygomorphy, an evolutionary novelty, by activating and repressing growth processes in dorsal petals and the dorsal stamen, respectively (Luo *et al.*, 1996). TCP-C genes belonging to the CINCINNATA (CIN) clade have a negative effect on cell proliferation during leaf development by modulating the switch from cell proliferation to cell differentiation, ensuring the formation of a plane leaf surface in *Antirrhinum* and *Arabidopsis* (Nath *et al.*, 2003; Palatnik *et al.*, 2003; Efroni *et al.*, 2008; Alvarez *et al.*, 2016). However, during petal development, *CIN* also activates cell proliferation in *Antirrhinum* (Crawford *et al.*, 2004). TCP-P genes were shown to function predominantly as positive growth regulators. *AtTCP14* and *-15* from *Arabidopsis* redundantly promote cell proliferation in young internodes; however, they also repress cell proliferation in leaf and floral tissues (Kieffer *et al.*, 2011). Thus, TCP genes can either promote or repress cell division depending on the given tissue or organ context.

TCP genes also gained attention for their impact on pigment synthesis in *Arabidopsis*. The TCP-C clade gene *AtTCP3*

*These authors contributed equally to this work.

enhances flavonoid synthesis in *Arabidopsis* seeds and seedlings (Li & Zachgo, 2013). On the other hand, the TCP-P gene *AtTCP15* restricts the expression of flavonoid biosynthesis genes, which occurs under short periods of high light. The repression is abolished under extended high light conditions, which is mediated by a redox-dependent modulation of the AtTCP15 protein activity, leading to the production of protective pigments and an adaptive stress response (Viola *et al.*, 2016).

During plant terrestrialization, likely *c.* 500 million yr ago (Ma) in the Cambrian–Early Ordovician period (Morris *et al.*, 2018), streptophyte ancestors of land plants were exposed to novel stresses, such as high irradiance, drought, and rapidly changing temperatures (de Vries & Archibald, 2018). In aquatic habitats of streptophytes, ultraviolet (UV) radiation is attenuated by water (H_2O), reducing exposure of harmful UV-B radiation (Maberly, 2014). UV-B light leads to the formation of reactive oxygen species (ROS), causing damage to membranes, proteins, and DNA (Hideg *et al.*, 2013), and the acquirement of traits conferring UV-B light resistance was advantageous for colonizing the new dry habitat. Land plants produce a broad range of protective secondary metabolites, particularly through the phenylpropanoid pathway (PPP; Vogt, 2010). The PPP generates a diverse group of flavonoids, and these antioxidants are known to function as ROS scavengers and as a sunscreen against UV-B radiation (Jansen *et al.*, 1998; Hideg *et al.*, 2013). TCP TFs emerged in streptophyte algae (Navaud *et al.*, 2007; Nishiyama *et al.*, 2018), which already possess several flavonoid synthesis genes (de Vries *et al.*, 2017). The genome of the basal land plant Marchantia encodes the core of flavonoid biosynthesis enzymes (Bowman *et al.*, 2017), and Marchantia was shown to form protective flavonoid pigments in response to stress (Albert *et al.*, 2018).

Whereas redundant TCP activities often hamper their analysis in angiosperms, genome analysis of the liverwort *Marchantia polymorpha* revealed the presence of only a single TCP-P (Mp*TCP1*) and TCP-C (Mp*TCP2*) gene in this basal land plant (Bowman *et al.*, 2017). We show that loss of Mp*TCP1* leads to decreased thallus growth through reduced cell proliferation, indicating a conserved, ancestral TCP-P function in growth regulation. In addition, Mp*TCP1* regulates a complex network of ROS producing and removing enzymes, modulating hydrogen peroxide (H_2O_2) levels. It is known that exposure to stress is often accompanied by reduced cell proliferation and retarded growth. ROS have long been recognized for their roles in mediating stress response and are recently gaining increasing attention for their roles in development (Schippers *et al.*, 2016; Mittler, 2017; Mhamdi & Van Breusegem, 2018; Noctor *et al.*, 2018; Waszczak *et al.*, 2018). The molecular mechanisms, governing stress and developmental processes, however, remain thus far largely unknown. Here, we demonstrate that loss of Mp*TCP1* activity leads to the accumulation of specialized and likely protective pigments, such as aminochrome (ac) and two derivatives. Together with an observed redox-dependent DNA binding of MpTCP1, our data suggest that MpTCP1 proteins can sense ROS changes and mediate adaptive regulatory responses to novel conditions experienced during the conquest of land.

Materials and Methods

Marchantia growth and transformation

Analyses were carried out with *M. polymorpha* ssp. *ruderalis*, ecotype BoGa, obtained from the Botanical Garden of Osnabrück, Germany. Sterile plant cultivation, induction of reproductive structures, and sporeling transformation were conducted according to Althoff *et al.* (2014).

Generation of transgenic knockout lines

A double CRISPR/Cas9 approach was carried out to delete *c.* 2.3 kb from the Mp*TCP1* locus, including the complete coding sequence (CDS; Supporting Information Fig. S1). Two synthetic guide RNAs (gRNA1, 5′-ATGAAACACTGGATAGCTG ATGG-3′, and gRNA2, 5′-GATTGGTTAAATGATAAGC GTGG-3′; Fig. S1), binding in the 5′ and 3′ untranslated regions (UTRs), respectively, were generated. Cloning was conducted as described (Sugano *et al.*, 2018) using pMpGE_En03, pMpGE010 for gRNA1, and pMpGE011 for gRNA2 (Addgene entry nos. 71535, 71536, 71537). *Agrobacterium*-mediated sporeling transformation was performed using both gRNA-containing vectors, and transgenic T_1 lines were screened via selection with 100 μg ml^{-1} cefotaxime, 10 μg ml^{-1} hygromycin, 0.5 μM chlorosulfuron, and sequencing. The three female lines Mp*tcp1-1*^{ge}, Mp*tcp1-2*^{ge} and Mp*tcp1-3*^{ge} were used for further analysis (Fig. S1).

RNA sequencing

For RNA sequencing (RNA-Seq), total RNA was isolated from 23-d-old wild-type and Mp*tcp1*^{ge} thallus as described in Busch *et al.* (2014). Library preparation, including polyA enrichment and sequencing of 150 nt paired-end reads on the Illumina HiSeq 3000-platform, was performed at the Max Planck Genome Center, Cologne. Sequence datasets were deposited at the Short Read Archive database at the National Center for Biotechnology Information under project PRJNA551935. Quality and adapter-trimmed paired-end reads were mapped to the *M. polymorpha* reference genome using STAR (v.2.5.3a). The read counts for each gene were estimated using RSEM (v.1.3.0). Reference genome and annotation were downloaded from marchantia.info. The R package DESEQ2 was used for statistical testing of pairwise comparison of the samples. Expression data are based on three independent wild-type lines and Mp*tcp1-1*^{ge}, Mp*tcp1-2*^{ge}, and Mp*tcp1-3*^{ge}. Functional annotation of gene accessions was downloaded from marchantia.info. Further analysis was done on differentially expressed genes (DEGs) with a minimum fold change of 2 and an adjusted *P*-value of < 0.0001 from comparisons of Mp*tcp1*^{ge} vs wild-type plants. Gene Ontology (GO) term enrichment analysis was conducted with AGRIGO v.2 (bioinfo.cau.edu.cn/agriGO/; Tian *et al.*, 2017) using standard settings. Significantly enriched GO terms (false discovery rate FDR < 0.05) were visualized as word cloud using WORDLE (www.wordle.net), where the weight of terms was defined as $-\log_{10}$ of the FDR.

In situ hybridization

For preparation of Mp*TCP1* antisense probe, a 2507 nt long PCR template was generated from thallus complementary DNA comprising the complete CDS. Mp*H4* (Mapoly0214s0009.1) template preparation and analysis of sections and whole mount tissue from 5-d-old gemmae were performed as described by Althoff *et al.* (2014) and Busch & Zachgo (2007). All primer sequences are given in Table S1.

Morphological analyses

For scanning electron microscopy, material was fixed (2% formaldehyde, 5% acetic acid, 54% ethanol) for 48 h at 4°C, washed, and dried in a series of increasing ethanol solutions. Material was critical-point dried in CO_2 using a CPD030 (Bal-Tec AG, Balzers, Liechtenstein) and sputter coated (K575X; Quorum Emitech, Quorum Technologies, Ringmer, UK). Microscopy was performed with a Zeiss Auriga scanning electron microscope. Pictures were taken from at least eight gemmae from three wild-type and Mp*tcp1*^{ge} plants after 0, 1, 5, 9 and 12 d of cultivation. Surface areas were measured with ImageJ (Fiji v.2.0.0-rc-59/1.51n) and mean values of each line were averaged. To measure the surface area of epidermal thallus cells, thallus pieces from 40-d-old plants were fixed (4% formaldehyde, 0.1 M phosphate buffer pH 7.2, 0.1% Tween-20) overnight, washed and cleared in 70% ethanol. Cell sizes were determined microscopically from thallus pieces, cut from the midrib region, adjacent to the first dichotomous branch-point, placed between a glass slide and cover slip. Average cell sizes are derived from Mp*tcp1-1/2/3*^{ge} and from two independent wild-type lines. For each line, cell sizes were measured from three plants, and averages are based on at least 200 cells per plant. Overall growth and cell size differences were statistically evaluated by Student's *t*-test using Spss v.23.0 (SPSS Inc., Chicago, IL, USA). For pigment visualization, thallus halves of 22-d-old plants were cleared with 70% methanol (MeOH). Pictures were taken with a Leica (Wetzlar, Germany) M165FC or CTR5000 and the DFC490 camera.

5-Ethynyl-2′-deoxyuridine staining

For detection of dividing nuclei, the Click-iT™ EdU Alexa Fluor™ 488 Imaging Kit (Life Technologies, Eugene, OR, USA) was used. The modified nucleoside 5-ethynyl-2′-deoxyuridine (EdU) was incorporated into DNA during S-phase and detected after covalent binding to a fluorescent dye. Nine-day-old gemmae from wild-type and Mp*tcp1*^{ge} lines, grown on ½ Gamborg medium on a cellophane disc, were processed as described by Furuya *et al.* (2018), without propidium iodide staining of cell walls. Stacks of images from apical notches were taken with the Zeiss Laser Scanning Microscope 510 META mounted with a ×10 objective. Images were taken from upper to lower sample surface with 2 µm increments. Nuclei were counted for each stack using the Imaris (v.9.2) spot counting tool. Average nuclei numbers are based on data from two wild-type and Mp*tcp1-2*^{ge} and Mp*tcp1-3*^{ge} lines. For each line, stained nuclei in apical notches were counted from thallus halves for a minimum of eight gemmae. Significances were estimated using Student's *t*-test.

Metabolome analysis

Three wild-type and Mp*tcp1-1/2/3*^{ge} lines were grown for 22 d under standard conditions and sampled in liquid nitrogen. For analysis of phenylpropanoids, ac, and ac derivatives, we used MeOH : H_2O (1 : 1) with 0.05% formic acid to extract red pigments. For each line, frozen plant material was ground in a Geno/Grinder (SPEX SamplePrep, Metuchen, NJ, USA) at 1100 rpm for 2 × 45 s and extracted with 1 µl extraction solution per milligram plant tissue (FW) in an ultrasound bath for 15 min at room temperature. For extraction of riccionidin (Fig. S2), the extraction solution was composed of 80% MeOH in water with 1% hydrochloric acid. All samples were analyzed using a high-performance liquid chromatography-diode array detector–high resolution mass spectrometry (HPLC-DAD–HRMS) system composed of an Agilent 1200 Series high-performance liquid chromatograph coupled to a Bruker maXis ESI-qTOF mass spectrometer. The chromatographic separation was carried out in an EC 250/4.6 mm Nucleodur Sphinx RP, 5 µm column (Macherey-Nagel, Düren, Germany), using H_2O with 0.1% formic acid (solvent A) and MeOH : acetonitrile (3 : 4) with 0.1% formic acid (solvent B). Two different approaches were used to analyze the extracts. For the metabolomic analyses of phenylpropanoids, ac, and ac derivatives, we used the following chromatographic gradient: 1.5–15% B in 16.5 min and 15–100% B until 56.5 min and ionization in both positive and negative modes. For detection of riccionidin (Fig. S2; Methods S1) the chromatographic separation was carried out using a shorter gradient: 30–100% of solvent B in 10 min and samples were analyzed in the positive mode.

H_2O_2 measurement and 3′-diaminobenzidine staining

A potassium iodide (KI) assay was conducted for colorimetric determination of the H_2O_2 content using the NanoPhotometer NP80 (Implen, München, Germany) (Junglee *et al.*, 2014). Three wild-type and Mp*tcp1-1/2/3*^{ge} lines were analyzed at 9 and 23 d after germination (DAG). For 3′-diaminobenzidine (DAB) staining, gemmae at 3 and 11 DAG were incubated in a 0.5 mg ml^{-1} DAB staining solution for 20 min on a rotary shaker, including 3 min preincubation under vacuum for gemmae at 11 DAG. Gemmae were washed in distilled H_2O immediately after incubation, with subsequent removal of Chl in 70% ethanol.

In vitro DNA binding assay

Protein generation and redox electrophoretic mobility shift assay (EMSA) studies were carried out according to Gutsche *et al.* (2017). Probes containing two repeats of site IIb (ACTCCATGGTCCCACCCATGGTCCCAC) and site IIa binding motifs (GGTGGGCCCGTAGGTGGGCCCGTA), similar to Kosugi & Ohashi (1997), and their mutagenized

versions, site ΔIIb (ACTCCATGGTCGAACCCATGGTCGAAC) and site ΔIIa (GGTGGGCGAGTAGGTGGGCGAGTA), were analyzed (binding motifs underlined). Purchased oligonucleotides are 5′ labeled with 6-carboxyfluorescin (Sigma-Aldrich). The CDS of Mp*TCP1* and Mp*TCP1C131S* were amplified with primers containing *Sal*I (5′) and *Hin*dIII (3′) restriction sites and cloned into the pMAL-c5X vector (New England Biotech, Ipswich, MA, USA), resulting in N-terminal fusions to the maltose binding protein (MBP). Exchange from Cys131 to serine (Ser) in MpTCP1C131S was generated with site-specific mutagenesis PCR using internal primers. Experiments were repeated at least three times using 500 ng of purified MpTCP1 protein added to 0.4 pmol of each DNA binding motif. Reducing sodium dodecyl sulfate polyacrylamide gel electrophoresis analysis was performed to ensure successful protein purification (Fig. S3; Methods S1).

Protein alignment

TCP-P sequences were obtained from databases provided by PHYTOZOME v.12.1 (phytozome.jgi.doe.gov), OneKP (db.cngb.org/onekp/), OrcAE (bioinformatics.psb.ugent.be/orcae), and MarpolBase (marchantia.info), and TCP domains were aligned manually. *Amborella trichopoda* Amtr_sc00069.147; *Arabidopsis thaliana* At1G69690; *Cosmarium subtumidum* Cs_WDGV 2052871; *Chara braunii* g6552; *Oryza sativa* LOC_Os 12 g07480.1; *Picea abies* Pa_contig25122; *Physcomitrella patens* Pp3c3_24664V3; *Selaginella moellendorffii* Sm_404061.

Results

Mp*TCP1* controls thallus growth

To analyze the function of the single TCP-P gene Mp*TCP1* from Marchantia (Bowman *et al.*, 2017), we generated Mp*tcp1*^{ge} knockout plants applying the CRISPR/Cas9 system (Sugano *et al.*, 2018). The Mp*TCP1* coding sequence was deleted using two guide RNAs that target the Mp*TCP1* locus in the 5′ and 3′ UTRs (Fig. S1a,b). Three knockout lines, Mp*tcp1-1*^{ge}, Mp*tcp1-2*^{ge} and Mp*tcp1-3*^{ge}, were further investigated, and all revealed stable phenotypes during several rounds of vegetative propagation. Mp*tcp1*^{ge} plants showed a reduced thallus growth compared with wild-type plants (Fig. 1a,b). The optical surface areas of developing gemmae were determined over the course of 0–12 DAG. Already at 0 DAG Mp*tcp1*^{ge} gemmae were 1.2-fold smaller than wild-type gemmae (Fig. 1c; Table S2). Compared with wild-type gemmae, the size difference increased during further development, and at 9 DAG and 12 DAG the Mp*tcp1*^{ge} gemmae were 2.4- and 3.3-fold smaller, respectively. Mutant thallus lobes start to bend upwards 12 DAG, impeding size determination at later stages.

By applying the transcription activator-like effector nucleases (TALEN) method (Kopischke *et al.*, 2017), additional Mp*tcp1*^{ge} mutants were generated that all show the same reduced thallus growth phenotype (Fig. S1c,d). Mp*tcp1*^{ge} lines expressing Mp*TCP1* under the ubiquitous *Marchantia elongation factor 1α* (Mp*EF1α*)-promoter (Althoff *et al.*, 2014) show a wild-type-like thallus growth (Fig. S1e), supporting a growth-promoting activity of Mp*TCP1*. To investigate whether this function is realized by modulation of cell size or cell division, epidermal thallus cell sizes were measured close to the first dichotomous branch point from 40-d-old Mp*tcp1-1/2/3*^{ge} lines and compared with those of two wild-type lines. Mp*tcp1*^{ge} plants formed *c.* 1.2-fold larger cells than wild-type lines (Fig. 1d; $2895 \pm 634\ \mu m^2$ vs $2447 \pm 509\ \mu m^2$), suggesting that smaller Mp*tcp1*^{ge} mutant thallus growth is caused through a difference in cell proliferation. To quantify cell division differences, S-phase cells in the apical notch, the area of meristematic activity, were visualized applying EdU staining (Furuya *et al.*, 2018) in two wild-type and Mp*tcp1*^{ge} lines. Microscopic analysis of EdU-stained meristematic regions was feasible in gemmae till 9 DAG, but thereafter it was hampered by increasing three-dimensional tissue complexity. Labelling of S-phase cells at 9 DAG is reduced in the apical notches of mutants compared with wild-type plants (Fig. 1f,g). Quantification of nuclear signals revealed that Mp*tcp1*^{ge} plants possess *c.* 2.4-times fewer dividing cells in the apical notch region (647 ± 35) than wild-type plants (1521 ± 135) do (Fig. 1e). Our data show that Mp*TCP1* has a positive effect on thallus growth through the promotion of cell proliferation.

Mp*TCP1* is expressed in the apical notch

To determine where Mp*TCP1* exerts its activity, the Mp*TCP1* mRNA expression pattern was detected and compared with that of *Histone 4* from Marchantia (Mp*H4*), a marker for S-phase cells (Althoff *et al.*, 2014). Serial thallus cross-sections through the apical notch region were hybridized with Mp*TCP1* and Mp*H4* antisense probes (Fig. 2a,b). Mp*TCP1* expression was detected in the apical notch (Fig. 2a) and overlaps with the area of Mp*H4* expression (Fig. 2b), revealing that Mp*TCP1* is expressed in meristematic regions with cell division activity. To visualize the expression pattern of Mp*TCP1* in intact apical notches, whole-mount *in situ* hybridization was performed on young gemmae at 5 DAG. The expression of Mp*TCP1*, as well as of Mp*H4*, encompasses the apical notch region (Fig. 2c,d), further supporting that Mp*TCP1* expression occurs in proliferating tissues. In gemma cups (Fig. 2e,f), Mp*TCP1* is strongly expressed in young and growing vegetative propagation units, the gemmae (Fig. 2e), and overlaps with Mp*H4* expression (Fig. 2f), indicating cell division activity. In older gemmae, where cell proliferation has likely ceased, Mp*TCP1* and also Mp*H4* expression decreases. Together, our *in situ* hybridization data support an Mp*TCP1* function in thallus growth promotion through a positive effect on cell proliferation in apical notches.

Mp*TCP1* exerts a function in archegoniophore development

To investigate the Mp*TCP1* function in reproductive structures, formation of archegoniophores, the female reproductive organs, was induced by far red light in the three female Mp*tcp1*^{ge} and three female wild-type lines. In wild-type archegoniophores, the

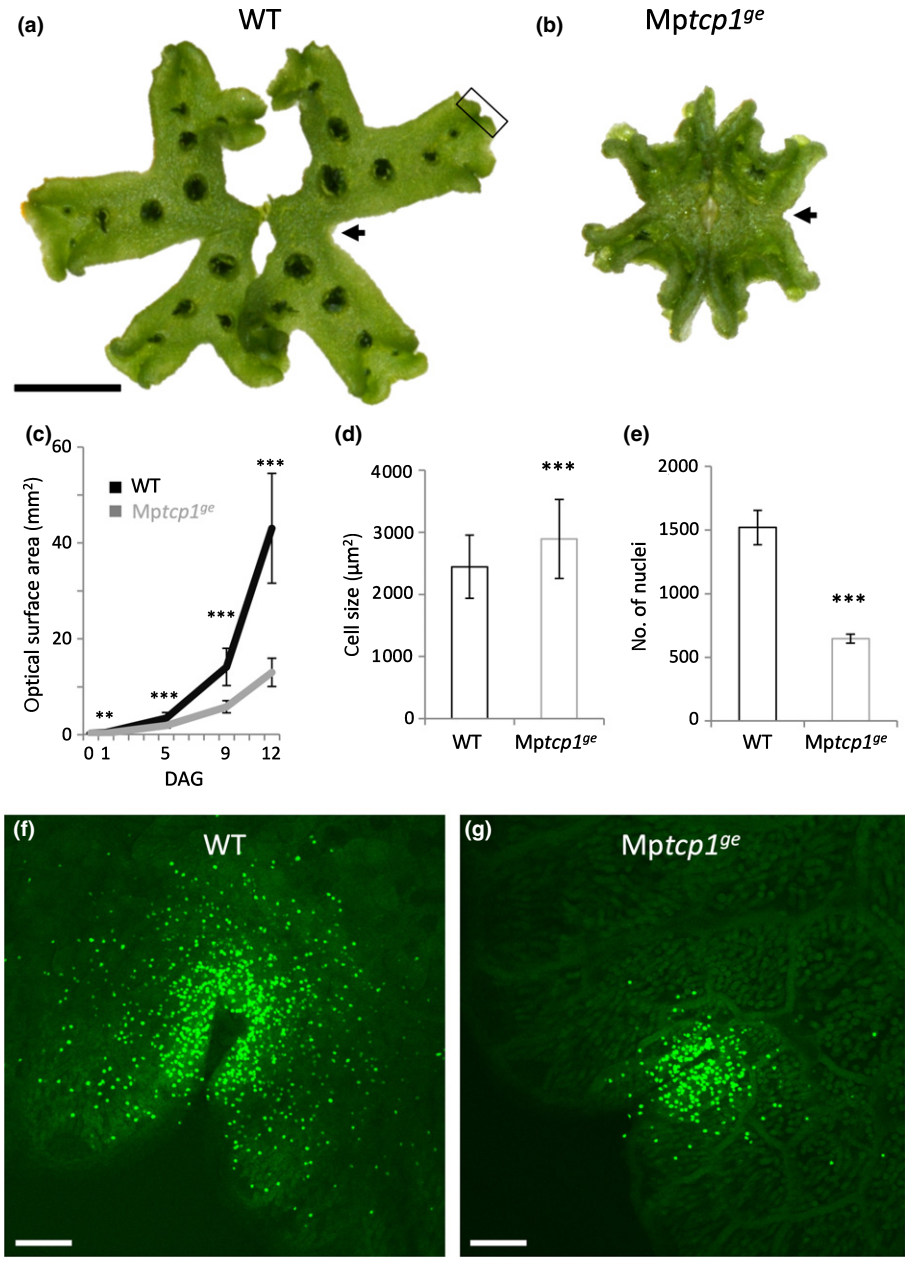

Fig. 1 Mp*TCP1* has a positive effect on thallus growth via promotion of cell proliferation in *Marchantia polymorpha*. Thallus of (a) wild-type (WT) and (b) Mp*tcp1-3*^{ge} plants 28 d after germination (DAG). The boxed region in (a) indicates an apical notch region. (c) The average surface area of complete gemmae was calculated from four WT and the three Mp*tcp1-1/2/3*^{ge} knockout lines after 0, 1, 5, 9, and 12 d of growth. (d) Average epidermal cell sizes of two WT and Mp*tcp1-1/2/3*^{ge} lines, measured adjacent to the first dichotomous branch point, indicated with an arrow in WT (a) and Mp*tcp1*^{ge} (b), at 40 DAG. (e) Proliferating cells were detected by 5-ethynyl-2′-deoxyuridine (EdU) staining of dividing nuclei in apical notches of gemmae at 9 DAG and counted. Representative projections of image stacks are shown from (f) WT and (g) Mp*tcp1-3*^{ge} EdU-stained apical notches. Bars: (a) 1 cm; (f, g) 100 µm. All error bars display ± SD, and *P*-values were determined by Student's *t*-test (**, $P < 0.01$; ***, $P < 0.001$).

capitulum forms about nine regularly shaped rays on an elongated stalk (Fig. 3a; Shimamura, 2016). Groups of archegonia are arranged between these rays at the bottom of the capitulum and are surrounded by involucres, a protective tissue (Fig. 3a,c,e). Contrarily, rays from Mp*tcp1*^{ge} archegoniophores are irregular in size and shape. The Mp*tcp1*^{ge} stalk length is reduced, and additional archegoniophores can develop beneath the rays (Figs 3b, inset, S4a,c). In early Mp*tcp1*^{ge} archegoniophore development, accessory tissue is formed at the bottom of the capitulum (Fig. 3d,f) that produces air pores (Fig. 3f, arrowhead), a dorsal characteristic. These tissues likely develop further into rays or additional archegoniophores. Abnormal archegoniophores bearing secondary archegoniophores have also been observed in natural *M. polymorpha* populations (Terui, 1975). Microtome sections support the observation that additional tissues form at the bottom of the Mp*tcp1*^{ge} capitula, enclosed in structures that resemble involucres (Fig. 3b). Differently from wild-type plants, pin-like structures can also emerge from the center of Mp*tcp1*^{ge} capitula (Fig. 3b, arrowheads). TALEN-generated Mp*tcp1*^{ge} plants develop similar archegoniophores (Fig. S4d). Antisense messenger RNA (mRNA) probes of Mp*TCP1* and Mp*H4* were hybridized to longitudinal sections of wild-type archegoniophores. Mp*TCP1* is expressed in the lower region of the capitulum tissue in a few cell layers above newly formed archegonia, proximal to the stalk (Fig. 3g). Mp*H4* transcript is also restricted to these cell layers, indicating regions of cell proliferation (Fig. 3h). Mutant phenotype and expression analysis imply that, in contrast to a positive role of Mp*TCP1* on thallus growth

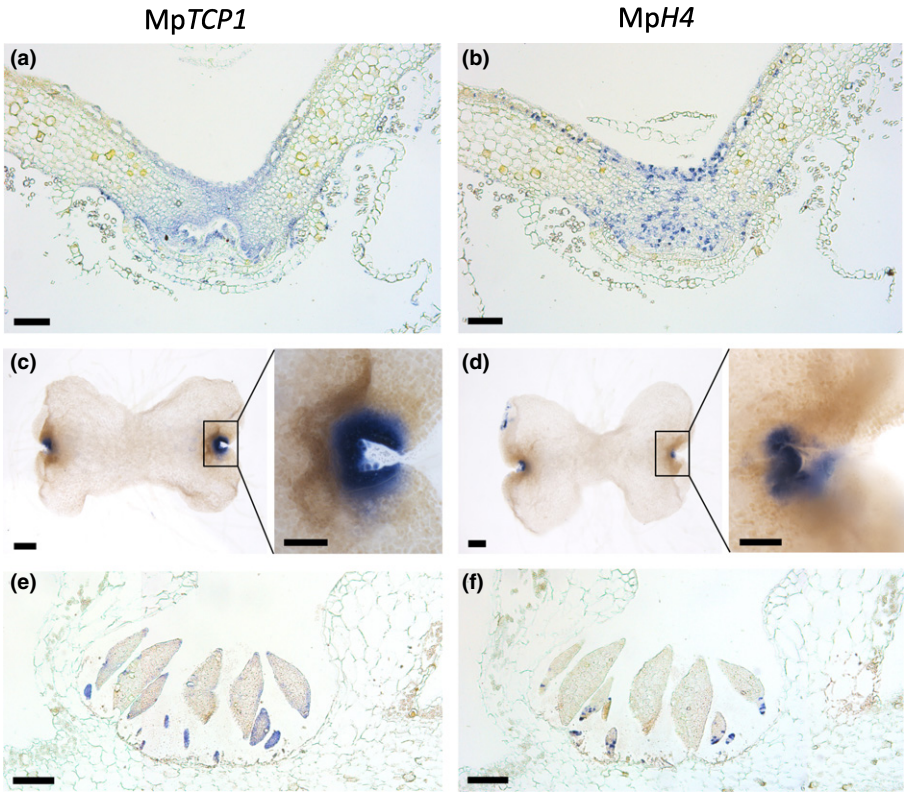

Fig. 2 Mp*TCP1* is expressed in regions of cell proliferation in vegetative tissue. (a, b) Serial cross-sections through apical notch regions of Marchantia thalli were hybridized with (a) Mp*TCP1* and (b) Mp*H4* antisense probes. (c, d) Whole mount *in situ* hybridization with 5-d-old gemmae detecting (c) Mp*TCP1* and (d) Mp*H4* expression. (e, f) Serial cross-sections through a gemma cup revealing (e) Mp*TCP1* and (f) Mp*H4* expression. Bars: (a, b, e, f) 100 μm; (c, d) 250 μm (insets, 100 μm).

through the promotion of cell proliferation, Mp*TCP1* restricts cell proliferation in female reproductive structures and prevents the development of extra archegoniophore tissue. In antheridiophores, the male reproductive structures, less severe developmental abnormalities were observed. Similar to mutant archegoniophores, stalk growth is reduced, and occasionally an extended growth of a few lobes (Fig. S4b,e,f) was observed, which is in compliance with a lower Mp*TCP1* mRNA expression during the development of these structures (Fig. S5).

Analysis of the Mp*TCP1*-controlled downstream network

To gain insight into the molecular processes controlled by Mp*TCP1*, we sequenced 23-d-old thallus transcriptomes from three wild-type and the three Mp*tcp1*^{ge} lines. Applying a fold change ≥ 2 and an adjusted *P*-value < 0.0001, 876 deregulated genes were identified, of which 426 genes were activated and 450 genes repressed by Mp*TCP1*.

Enriched GO terms were determined to detect commonalities amongst the DEGs. This identified in the category *biological process* the GO term *oxidation reduction process* as the most significantly enriched DEG group (Fig. 4a), which comprises several genes with a known activity in H_2O_2 metabolism and transport (Tables 1, S3a). H_2O_2 is a key ROS and potentially toxic, but there is growing support that H_2O_2 exerts crucial roles in signaling and also in developmental processes (Tsukagoshi, 2016; Mittler, 2017; Mhamdi & Van Breusegem, 2018; Waszczak *et al.*, 2018). The largest group of DEGs comprises class III peroxidases (PRXs), the expression of 25 of these PRXs being downregulated and seven being upregulated by Mp*TCP1* activity. Apoplastic class III PRXs are key antioxidant enzymes that reduce H_2O_2 molecules to H_2O. However, substrate dependently, they also generate superoxide radicals ($O_2^{\bullet -}$), which can spontaneously dismutate to H_2O_2 (Francoz *et al.*, 2015; Shigeto & Tsutsumi, 2016). Additionally, a copper-containing amine oxidase and two polyamine oxidases, known to generate H_2O_2 (Tavladoraki *et al.*, 2016), are upregulated in Mp*tcp1*^{ge} mutants. Expression of a single catalase (CAT) gene, known to be an integral part of the plant antioxidative system for conducting the dismutation of H_2O_2 to water (Mhamdi *et al.*, 2010), is approx. nine-fold repressed. Furthermore, two dehydroascorbate reductases (DHARs), which constitute a class of glutathione *S*-transferases counteracting oxidizing conditions (Dixon & Edwards, 2010) are downregulated. Besides these enzymes involved in ROS metabolism, a group of nine aquaporin transporters, comprising plasma membrane intrinsic protein and tonoplast intrinsic protein homologues, are between *c.* 2- and *c.* 21-fold upregulated in Mp*tcp1*^{ge} lines. Aquaporins not only mediate the transport of H_2O across cell membranes but also facilitate the diffusion of H_2O_2 into the cytoplasm (Hooijmaijers *et al.*, 2012; Bienert & Chaumont, 2014).

Comparison of H_2O_2 levels by KI staining of 12- and 23-d-old wild-type and Mp*tcp1*^{ge} thalli detected an increased H_2O_2 content in mutant thalli (Fig. 4b). Additional H_2O_2 visualization by DAB staining identified a stronger staining in Mp*tcp1*^{ge} gemmae at 3 and 11 DAG compared with wild-type lines, including the apical notches, where Mp*TCP1* mRNA expression was detected (Fig. 2c,d). In order to determine whether increased

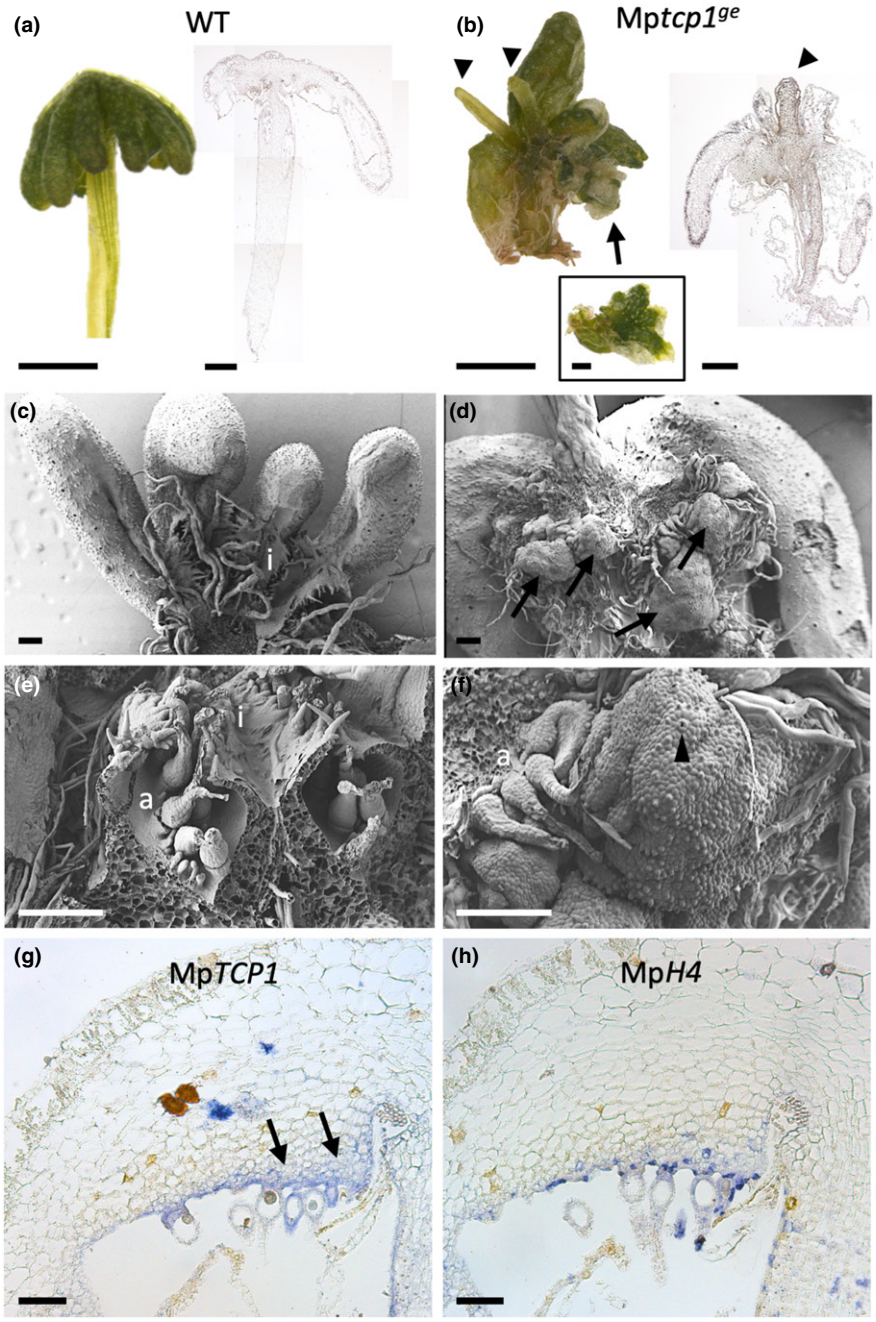

Fig. 3 Mp*TCP1* affects Marchantia archegoniophore development. (a) Wild-type (WT) capitulum where the lower part of the stalk was removed from the archegoniophore (left) and a longitudinal section through a complete archegoniophore (right). (b) Mp*tcp1-3*^{ge} archegoniophore with irregularly formed rays (left), where one ray was removed to exhibit a secondarily formed archegoniophore (arrow) shown in the inset and longitudinal section through Mp*tcp1-3*^{ge} archegoniophore (right). Pin-formed tissue can emerge from the dorsal center of the capitulum (arrowheads) that is formed on a truncated stalk. (c–f) Scanning electron microscope images of WT and Mp*tcp1-3*^{ge} archegoniophores. (c) Bottom view of WT capitulum with involucres enclosing archegonia. (d) Side view on Mp*tcp1-3*^{ge} capitulum. Some rays were removed to visualize additionally formed tissue, indicated by arrows. (e) WT archegonia developing between two rays, enveloped in involucres. (f) Close-up of (d) showing newly emerged tissue that forms air pores (arrowhead). (g, h) Serial longitudinal sections through WT archegoniophores were hybridized with (g) Mp*TCP1* and (h) Mp*H4* antisense RNA probes. Arrows indicate Mp*TCP1* expressing cell layers. a, archegonia; i, involucre. Bars: (a, b) 2 mm (left), 500 μm (right), 500 μm (inset); (c–f) 200 μm; (g, h) 100 μm.

H_2O_2 levels cause a thallus growth response in wild-type plants, gemmae were cultivated on medium supplemented with 3-amino-1,2,4-triazole (3-AT) till 9 DAG. 3-AT is known to specifically block catalase activity (Havir, 1992; Zeng *et al.*, 2017) and caused a 1.9-fold H_2O_2 increase in these gemmae (Fig. S6a). In addition, we determined a growth defect, as 3–17 DAG the gemmae reveal a 1.7- to 2.3-fold size reduction compared with untreated gemmae of the same age (Fig. S6b; Table S4). These data indicate that elevated H_2O_2 levels exert a negative effect on thallus growth. Together, these observations support a function for Mp*TCP1* in maintaining a proper ROS balance required for normal Marchantia thallus growth and development. Comparison of archegoniophore transcriptomes and H_2O_2 levels did not indicate a participation of redox processes in governing the overproliferation phenotype observed in archegoniophores (Fig. S7a).

Mp*TCP1* represses violet pigment production in the thallus

When grown under standard light conditions, Mp*tcp1*^{ge} plants produce violet pigment along the ventral midrib region, which was barely visible in wild-type plants (Fig. 5a). We hypothesized that this pigment could be related to riccionidin, an anthocyanidin, whose synthesis has been shown to be enhanced under stress

conditions (Albert *et al.*, 2018). The red pigment produced in Mp*tcp1*^{ge} plants was recovered and analyzed by HPLC-DAD–HRMS (Fig. 5b). In a UV chromatogram, three peaks were higher in Mp*tcp1*^{ge} than in wild-type plants (Fig. 5b). UV spectra related to these peaks revealed a maximum absorption at *c.* 300 nm (Fig. 5c), suggesting that the compounds are unlikely related to riccionidin (Kunz *et al.*, 1994; Albert *et al.*, 2018). Additionally, molecular masses of the three major compounds (*m*/*z* 166.0865, 150.0551, 180.0657; Fig. 5c; Table S5) were much smaller than expected for riccionidin (Kunz *et al.*, 1994; Albert *et al.*, 2018) (see Fig. S2). The UV profiles and mass ranges are very similar to tyrosine oxidation products reported by Dagnino-Subiabre *et al.* (2000) and Cui *et al.* (2017). Based on the UV absorbance and HRMS data, we propose that the compound related to peak 2 is aminochrome (ac), a tyrosine oxidation product, and compounds related to peaks 1 and 3 are ac derivatives, which we accordingly refer to as ac-derivative 1 and ac-derivative 3. Relative quantification revealed that ac, ac-derivative 1, and ac-derivative 3 are 8.9-, 11.0- and 13.2-fold, respectively, more abundant in Mp*tcp1*^{ge} than in wild-type thalli (Fig. 5d; Table S5). Thus, Mp*TCP1* represses the synthesis of ac and its derivatives, which have known functions in the formation of neuromelanine in animals (Munoz *et al.*, 2012), but to date no function has been described for these compounds in plants. In walnut, levels of the ac derivative 5,6-dihydroxyindole significantly decreased upon silencing of the single polyphenol oxidase (PPO; Araji *et al.*, 2014), a copper-containing enzyme capable of monophenol hydroxylation to *o*-diphenols as well as oxidation of *o*-diphenols to *o*-quinones (Li *et al.*, 2010; Araji *et al.*, 2014; Solano, 2014). PPOs are involved in ac synthesis by oxidation of the phenolic tyrosine ring, the starting substrate in this reaction.

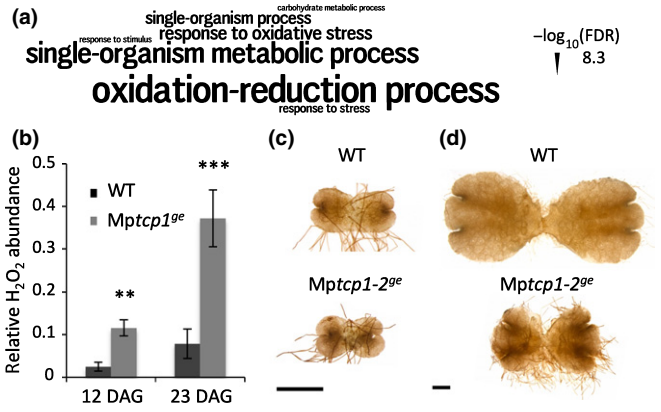

Fig. 4 Mp*TCP1* regulates redox processes in *Marchantia polymorpha*. (a) Gene Ontology (GO) enrichment word cloud (category *biological process*) of deregulated genes detected by thallus transcriptome comparison (fold change ≥ 2; adjusted *P*-value < 0.0001) between 23 DAG Mp*tcp1*^{ge} and wild-type (WT) plants. Font size corresponds to significance of GO terms. FRD, false discovery rate. (b) Determination of hydrogen peroxide (H_2O_2) in extracts from 12 and 23 DAG WT and Mp*tcp1*^{ge} thalli using potassium iodide staining. Average values are derived from three independent measurements of three WT and the three Mp*tcp1*^{ge} lines. Error bars display ± SD, and *P*-values were determined by Student's *t*-test (**, $P < 0.01$; ***, $P < 0.001$). (c, d) Visualization of H_2O_2 by 3′-diaminobenzidine staining in gemmae of WT and Mp*tcp1-2*^{ge} plants at (c) 3 DAG and (d) 11 DAG. Bars, 1 mm.

The increased amount of these three acs in Mp*tcp1*^{ge} plants is in line with the observed three- to even 335-fold upregulation of 20 PPOs in Mp*tcp1*^{ge} mutants (Tables 1, S3a). The HRMS, UV, and transcriptomic data strongly suggest that the red pigments are related to acs. A definite chemical identification of these pigments could be achieved by NMR studies or comparison with standards. Comparative HPLC-DAD–HRMS analyses show that riccionidin is not present in high amounts in Mp*tcp1*^{ge} thallus and, thus, likely does not make a major contribution to the observed red pigmentation phenotype of the mutants (Fig. S2).

Furthermore, we detected an increase of three additional compounds, which absorb light between 280 and 340 nm and likely derive from the phenylpropanoid pathway (PPP) (Table S5). Supportively, RNA-Seq analysis detected three upregulated genes encoding for relevant enzymes in Mp*tcp1*^{ge} plants (Tables 1, S3a): 3-deoxy-D-arabino-heptulosonate-7-phosphate synthase, an enzyme from the shikimate pathway, feeds the starting substrate phenylalanine into the PPP; a cinnamate 4-hydroxylase, which catalyzes the aromatic hydroxylation to form 4-coumarate in flavonoid biosynthesis (Vogt, 2010); and a member of the Marchantia chalcone synthase (CHS) family, whose single homologue *TRANSPARENT TESTA 4* in *Arabidopsis* catalyzes the committing step of flavonoid biosynthesis (Yin *et al.*, 2012). Our metabolic analysis proposes that Mp*TCP1* represses the formation of a comprehensive portfolio of pigments and secondary compounds from different metabolic pathways in the thallus, amongst them even some that are not commonly observed in plants. In Mp*tcp1*^{ge} archegoniophores, no pigment formation was observed (Fig. S7b). One CHS and one PPO were downregulated upon loss of Mp*TCP1* (Fig. S7c), indicating, as described for the growth control, a tissue-dependent Mp*TCP1* regulatory activity.

MpTCP1 proteins bind DNA redox dependently

Given our observation that Mp*TCP1* regulates genes involved in redox regulation processes, we investigated whether the DNA binding capacity of the MpTCP1 protein is also redox regulated. Recently, Viola *et al.* (2013) identified a conserved cysteine (Cys) at the start of the first helix in the TCP domain of TCP-P proteins and demonstrated that the respective Cyses of several *Arabidopsis* TCP-P proteins mediate a redox-sensitive DNA binding. A comparison of TCP-P domain sequences from evolutionary informative representatives including algae, basal plants, and higher land plants (Fig. 6a) also identified a conserved Cys in MpTCP1 at amino acid position 131 (Cys131, Fig. S1a). It was shown earlier that the TCP domain mediates binding of TCP TFs to conserved DNA recognition elements, so-called site IIa and site IIb motifs (Kosugi & Ohashi, 1997, 2002). We performed EMSAs to investigate whether the Marchantia TCP-P also binds to the consensus TCP binding sites and to determine the effects of redox changes. MpTCP1 proteins were expressed in *Escherichia coli* as fusion proteins with the MBP, lacking Cys residues. We tested fluorophore-labeled probes comprising two site IIb and two site IIa binding motifs in addition to their respective mutagenized versions (Fig. 6b) (Kosugi & Ohashi,

Table 1 Genes regulated by Mp*TCP1*.

Annotation	No. of DEGs	FC range (Mp*tcp1*^{ge}/WT)	Putative metabolic function
PRXIII	25	2.3 to 20.7	Apoplastic generation and degradation of H_2O_2 in a substrate-dependent manner and oxidative
	7	−76.3 to −2.4	Coupling of monolignols, precursors in lignan/lignin biosynthesis
Catalase	1	−8.5	Dismutation of H_2O_2 to H_2O
Copper amine oxidase	1	12.4	Source of H_2O_2
Polyamine oxidase	2	2.3, 2.5	Source of H_2O_2
Glutathione-*S*-transferase (DHAR)	2	−5.1, −4.9	Reduction of dehydroascorbate and concomitant oxidation of GSH to GSSG
Aquaporins	9	2.4 to 20.7	Transport of H_2O and H_2O_2 across cell membrane into the cytoplasm
Dirigent-like proteins	1	−5.9	Ensure stereoselectivity of monolignol coupling in lignan/lignin biosynthesis
	8	2.1 to 65.2	
PPO/tyrosinases	20	3.1 to 334.8	Synthesis of aminochrome and derivatives by oxidizing the phenolic ring of tyrosine
Chalcone synthase	1	4.6	PPP enzyme; synthesis of chalcone, a key step in flavonoid biosynthesis
C4H	1	3.0	PPP enzyme; catalysis of the aromatic hydroxylation forming 4-coumarate
DAHPS	1	2.0	Enzyme of the shikimate pathway, which provides phenylalanine to the PPP

Determination of differentially expressed genes (DEGs) by comparing Mp*tcp1*^{ge} and wild-type (WT) Marchantia thallus transcriptomes (fold change (FC) ≥ 2; adjusted *P*-value < 0.0001) reveals an Mp*TCP1* function in regulating a reactive oxygen species metabolism network and genes involved in secondary metabolite synthesis, such as pigment formation. Putative gene functions are based on Marchantia functional gene annotations, downloaded from marchantia.info and/or sequence comparison with *Arabidopsis thaliana* using Blast v.2.2.8 provided by The Arabidopsis Information Resource (www.arabidopsis.org/index.jsp). A list with all accessions from the gene groups mentioned is given in Supporting Information Table S3(a).
C4H, cinnamate 4-hydroxylase; DAHPS, 3-deoxy-D-arabino-heptulosonate-7-phosphate synthase; DHAR, dehydroascorbate reductase; GSH, glutathione; GSSG, oxidized glutathione disulfide dimer; H_2O, water; H_2O_2, hydrogen peroxide; PPO, polyphenol oxidase; PPP, phenylpropanoid pathway; PRXIII, class III peroxidase.

1997). Whereas the MBP protein alone does not interact with the motifs, MpTCP1 binds to site IIa and site IIb motifs. For both motifs, nucleotide exchanges in the core binding sites abolish an interaction with DNA (Fig. 6c), supporting specificity of MpTCP1 binding. Next, binding sensitivity of MpTCP1 was tested under different redox conditions. MpTCP1 was incubated with a reducing (0.9 mM dithiothreitol (DTT)) or oxidizing (2 mM diamide) reagent before incubation with the motifs. MpTCP1 binds to both motifs under reducing conditions, whereas oxidizing conditions abolished interactions (Fig. 6d), which could be reversed under highly reducing conditions (20 mM DTT; Fig. 6d). The impact of Cys131 on the redox-dependent binding of MpTCP1 was determined by replacing Cys131 by a Ser (MpTCP1C131S). MpTCP1C131S was no longer sensitive to altered redox changes and bound to both motifs under reducing and oxidizing conditions (Fig. 6e). Our data support a redox modulation of the MpTCP1 protein activity, which affects its DNA binding capacity and is mediated by a highly conserved Cys in the TCP domain.

Discussion

The TCP-P TF Mp*TCP1* regulates cell proliferation context dependently

TCP genes are key regulators known to control cell proliferation in angiosperms, for which the classical assumption has been that TCP-P genes promote and TCP-C genes repress cell proliferation. Here, we show that the single TCP-P gene Mp*TCP1* exerts a context-dependent regulatory function in the basal land plant *M. polymorpha*. Mp*TCP1* promotes cell proliferation in apical notches, meristematic areas of vegetative thallus tissues. Contrarily, during reproductive organ development, Mp*TCP1* represses tissue proliferation. Several angiosperm studies have shown a context-dependent TCP regulatory capacity. The TCP-C *CIN* gene from *Antirrhinum* conversely controls cell division of petals and leaves (Nath *et al.*, 2003; Crawford *et al.*, 2004). Likewise, the *Arabidopsis* TCP-P genes *AtTCP14* and *-15* promote cell division in young inflorescence internodes and embryos, whereas they repress proliferation in developing leaves (Kieffer *et al.*, 2011) and similarly, *AtTCP20* overexpression studies also support context-dependent TCP-P activities (Herve *et al.*, 2009). Angiosperm TCP proteins are known to bind to DNA as dimers and predominately interact with members from their own TCP group (Kosugi & Ohashi, 2002; Danisman *et al.*, 2013). However, interactions with non-TCP TFs can also affect TCP functions (Li & Zachgo, 2013; Wang *et al.*, 2015; Guan *et al.*, 2017) and provide a means to alter the outcome of the regulatory Mp*TCP1* capacities in different developmental stages. Together, context-dependent differences in the mode of cell proliferation control by TCP-P already exists in liverworts, one of the earliest diverging land plants, and could therefore have contributed to the diversification of embryophyte body plans.

Mp*TCP1* controls a redox network

Interestingly, and thus far not reported by comprehensive angiosperm TCP analyses, loss of Mp*TCP1* activity affects the expression of several groups of enzymes involved in ROS metabolism. Plant-specific class III PRXs that are up- and down-regulated in knockout plants not only can catalyze the

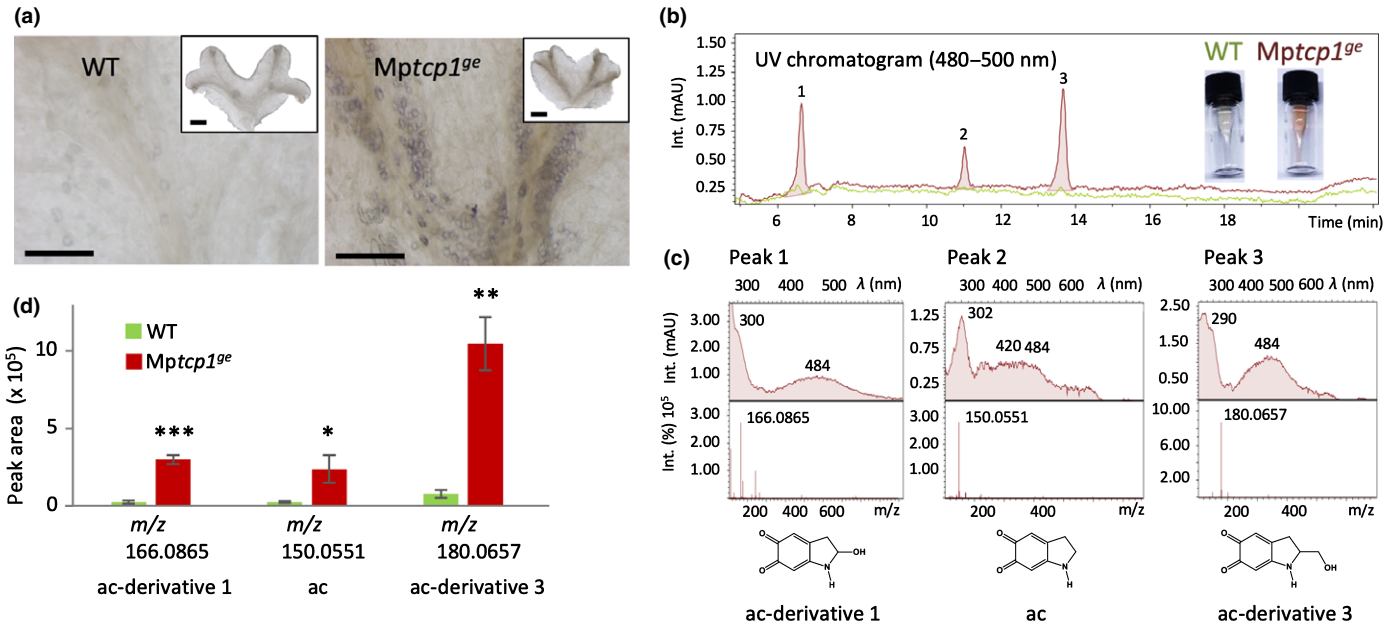

Fig. 5 Mp*TCP1* controls the accumulation of aminochrome (ac) and ac-derivatives 1 and 3. (a) Images of Marchantia wild-type (WT) and Mp*tcp1-1*^{ge} ventral midrib regions taken from thallus 22 d after germination (inset) after clearing. Bars, 500 μm (insets 2 mm). (b, c) High-performance liquid chromatography-diode array detector–high resolution mass spectrometry analysis of WT and Mp*tcp1*^{ge} Marchantia plants. (b) Ultraviolet (UV) chromatogram at 480–500 nm of Mp*tcp1*^{ge} (red line) and WT (green line) plants detected three stronger peaks in mutant plants. Extracts from WT and Mp*tcp1*^{ge} thalli are shown top right. (c) The three peaks (1, 2 and 3) from Mp*tcp1*^{ge} plants were further analyzed using UV (top) and MS spectra (bottom). The chemical structures determined are given underneath and resemble ac (peak 2) and ac-derivatives (peaks 1 and 3). (d) Relative quantification of the three compounds according to their exact masses (*m/z* 166.0865, *m/z* 150.0551, *m/z* 180.0657) based on selected ion chromatography of three WT and three Mp*tcp1*^{ge} plants. Error bars display ± SD, and *P*-values were determined by Student's *t*-test (*, $P<0.05$; **, $P<0.01$; ***, $P<0.001$). λ, wavelength; *m/z*, mass divided by charge number of ions; Int., Intensity; mAU, milli-absorbance units.

dismutation of H_2O_2 to H_2O in the apoplast (Francoz *et al.*, 2015; Shigeto & Tsutsumi, 2016) but also generate H_2O_2 via $O_2^{\cdot-}$ production, as shown for the liverwort *Dumortiera hirsuta* (Li *et al.*, 2010). The promotion or restriction of cell expansion through class III PRX in *Arabidopsis* seems to be dependent on the H_2O_2 level in the surrounding environment (Lu *et al.*, 2014). Additionally, a copper-containing amine oxidase and two polyamine oxidases, also sources for apoplastic H_2O_2 production, are upregulated in Mp*tcp1*^{ge} plants (Tavladoraki *et al.*, 2016). We identified one downregulated CAT, an ancient H_2O_2 scavenger, dismutating H_2O_2 to H_2O and oxygen (Mhamdi *et al.*, 2010). Similar to Mp*tcp1*^{ge} plants, the *Arabidopsis cat2* mutant shows a decreased growth rate, coinciding with the induction of H_2O_2-responsive transcripts (Queval *et al.*, 2007). Furthermore, decreased expression of two DHARs, catalyzing the reduction of dehydroascorbate to ascorbate with the concomitant oxidation of glutathione to oxidized glutathione disulfide (Dixon & Edwards, 2010), could contribute to enhance oxidizing conditions in Mp*tcp1*^{ge} thalli. The opposing regulation of H_2O_2-producing and H_2O_2-degrading enzymes by Mp*TCP1* likely together contributes to increased H_2O_2 levels in Mp*tcp1*^{ge} mutants. Additionally, the expression of nine aquaporins, integral membrane proteins, was increased up to 21-fold in Mp*tcp1*^{ge} mutants. Plant aquaporins facilitate not only H_2O but also H_2O_2 translocation, namely in developmental processes such as seed germination and lateral root emergence, as well as during pathogen defense (Dynowski *et al.*, 2008; Bienert & Chaumont, 2014; Maurel *et al.*, 2015; Tian *et al.*, 2016). By facilitating H_2O_2 transport into the cytoplasm, aquaporins could close the cytological gap between apoplastically generated H_2O_2 through upregulated PRXs and an intracellular H_2O_2 performance. Increased cytoplasmic H_2O_2 levels can then trigger signaling processes and posttranslational protein modifications. The spatiotemporal regulation of H_2O_2 and $O_2^{\cdot-}$ levels has recently been shown to control the balance between cell proliferation and differentiation processes in *Arabidopsis* shoot and root meristems (Tsukagoshi *et al.*, 2010; Zeng *et al.*, 2017). The reduced cell proliferation in the Mp*tcp1*^{ge} thallus could therefore be a consequence of misbalanced ROS levels, which is consistent with the observation that the inhibition of catalases results in a reduced Marchantia thallus growth. Here, similar to *Arabidopsis*, increased H_2O_2 levels might promote a switch from cell proliferation to cell differentiation processes. Differently, during archegoniophore development, loss of Mp*TCP1* activity leads to an overproliferation phenotype, which is independent of an altered ROS status, indicating a context-dependent ROS regulation. Together with the observation that aquaporins exert a function in osmoregulation, as overexpression of a ginseng aquaporin in *Arabidopsis* was associated with leaf cell expansion (Lin *et al.*, 2007), this might also explain the slight increase of epidermal cell sizes in Mp*tcp1*^{ge} thalli.

Together, these data indicate that Mp*TCP1* affects a complex ROS metabolic network that already exists in early diverging land

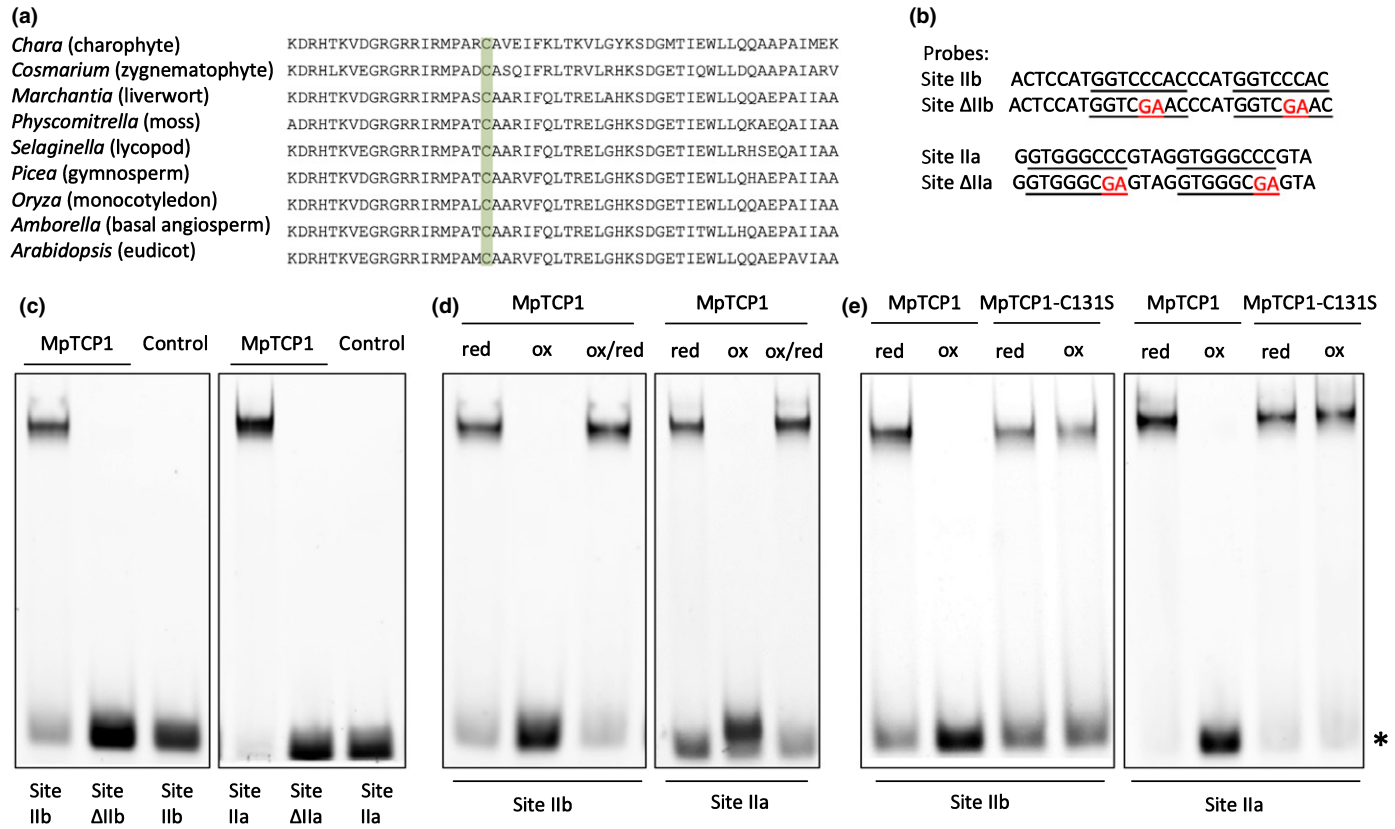

Fig. 6 MpTCP1 DNA binding studies. (a) TCP-domain alignment of TCP-P transcription factors (TFs) from evolutionary informative plant species. All TCP-P proteins analyzed share a conserved cysteine (Cys) in the DNA-binding TCP domain, indicated in green. (b) DNA-probe sequences contain either two site IIa or site IIb DNA binding sites (underlined) (Kosugi & Ohashi, 1997). Mutagenized nucleotides in site ΔIIa and site ΔIIb probes known to abrogate DNA binding of angiosperm TCP TFs are indicated in red. (c) Electrophoretic mobility shift assay (EMSA) analyses were conducted with maltose binding protein (MBP)-MpTCP1 fusion proteins, and MBP protein was applied alone as control. (d) Redox-dependent MpTCP1 binding analysis under reducing (red, 0.9 mM dithiothreitol (DTT)) and oxidizing (ox, 2 mM diamide) conditions and after reversing oxidizing conditions by addition of 20 mM DTT (ox/red). (e) Redox EMSA to determine the impact of the conserved Cys using MpTCP1C131S, where Cys131 was mutagenized to serine. Asterisk marks unbound free DNA probe.

plants and likely contributes to the coordination of cell proliferation and differentiation processes.

Mp*TCP1* controls the formation of novel plant pigments

We detected the accumulation of a violet pigment on the ventral thallus that comprises three compounds resembling ac and two derivatives. Biosynthesis of acs from tyrosine is catalyzed by the activity of PPOs, also referred to as tyrosinases (Remiao *et al.*, 2003; Munoz *et al.*, 2012; Araji *et al.*, 2014; Solano, 2014; Sugumaran, 2016). In strong correlation, RNA-Seq analysis detected 20 PPOs, where expression levels were enhanced up to *c.* 335-fold in Mp*tcp1*^{ge} lines. In angiosperms, PPOs have been shown to be involved in stress responses (Constabel & Ryan, 1998; Li & Steffens, 2002; Thipyapong *et al.*, 2004) and might contribute to the formation of ROS (Komarov *et al.*, 2005; Li *et al.*, 2010). As pigments, acs absorb light of two wavelengths, *c.* 300 and 480 nm, and might therefore render protection from UV-B radiation with wavelength band ranges from 280 to 320 nm (Hideg *et al.*, 2013). Acs can polymerize to form melanin and, in the case of animal neural cells, also neuromelanin, which both function in protection from oxidative stress. Melanin is believed to function as a photoprotectant and might play a role in plant resistance to pathogens (Bell, 1981; Bindoli *et al.*, 1992; Munoz *et al.*, 2012; Solano, 2014). Acs thus present a novel group of plant metabolites that could be involved in specialized protective mechanisms in Marchantia. In addition to controlling ac synthesis, metabolome and transcriptome analyses also support a function for Mp*TCP1* in repressing the production of three phenylpropanoid-derived compounds that similarly absorb light in the UV-B range and that might, thus, also exhibit protective functions. Furthermore, as oxidative enzymes, class III PRXs catalyze lignin and lignan production, where stereoselectivity is conferred by dirigent (DIR) and DIR-like proteins, of which eight were identified as being upregulated in Mp*tcp1*^{ge} thalli (Table 1). Lignin and lignans perform roles in secondary metabolism and defense responses (Li *et al.*, 2017; Paniagua *et al.*, 2017).

Several hundred new chemical compounds have been isolated from bryophytes, and Marchantia in particular accumulates significantly more unique secondary metabolites than other bryophytes analyzed (Asakawa *et al.*, 2013; Peters *et al.*, 2018). Our data show that Mp*TCP1* is a regulator of a comprehensive

array of specialized secondary metabolites, which likely confer protection against diverse abiotic and biotic stress factors and/or directly scavenge ROS.

Redox control of the MpTCP1 protein activity

EMSAs demonstrate a redox-dependent DNA interaction of MpTCP1 proteins. Whereas oxidizing conditions abolish an interaction, binding under reducing conditions is mediated via the exclusive Cys131, located in the first helix of the MpTCP1 TCP domain. For the *Arabidopsis* TCP-P protein AtTCP15, it was recently shown that redox changes induced through prolonged periods of high light abolish DNA binding of AtTCP15 to enable anthocyanin production as an adaptation to light stress (Viola *et al.*, 2016). The authors suggested that oxidizing conditions are associated with the formation of an intermolecular disulfide bond between the two conserved TCP domain Cyses, which affects TCP dimer conformation such that DNA binding is no longer possible. Our data propose a posttranslational, redox-regulated modulation of the single TCP-P protein activity in Marchantia thallus tissue, likely through similar conformational changes hindering DNA binding. This provides a means by which MpTCP1 proteins can sense altered redox conditions, such as imbalanced H_2O_2 levels generated in response to environmental changes. Modulation of the MpTCP1 DNA interaction can then rapidly mediate an adaptive transcriptome response by regulating the synthesis of protective secondary metabolites. Reversibility of a redox-regulated TF activity has been observed for BRASSINAZOLE-RESISTANT1, a key regulator in brassinosteroid signaling, whose activity is enhanced by H_2O_2-mediated oxidation and diminished after reduction via interaction with the thioredoxin TRXh5 (Tian *et al.*, 2018). For animals, the crucial role of H_2O_2 in signaling and growth control is well established. Recently, it also became an emerging perspective for angiosperm development (Tsukagoshi, 2016; Waszczak *et al.*, 2018), and the role of redox regulation of TFs is gaining increasing attention (Dietz, 2014; He *et al.*, 2018). Our characterization of Mp*TCP1* suggests that redox processes and balanced ROS signaling are important for the regulation of growth control of early diverging land plants. Given the presence of a single, conserved TCP-P Cys in charophycean algae and land plants, this Cys might already have contributed to sensing and responding to redox changes in water-living algae. Early diverging land plants, however, lost the protective buffering capacities of water and, thus, encountered increased and more variable abiotic stresses. Preexisting redox sensing and redox protection mechanisms could have contributed to an acclimation to environmental changes. The identification of key regulatory TFs, such as the single TCP-P gene Mp*TCP1* analyzed here, provides, together with the recent advances in ROS sensor and proteomic tool generation (Smirnoff & Arnaud, 2019), access to deepen our understanding of the impact of redox-regulated processes. Future studies will shed light on the mechanisms that allowed coping with novel challenges accompanying terrestrialization over 500 Ma and will elucidate how redox-controlled cell division and differentiation processes contributed to the diversification and increasing complexity of land plants.

Acknowledgements

Bioinformatics support by the BMBF-funded project 'Bielefeld-Gießen Center for Microbial Bioinformatics - BiGi (grant no. 031A533)' within the German Network for Bioinformatics Infrastructure (de.NBI) is gratefully acknowledged. We thank Claudia Gieshoidt for Marchantia tissue culture support and Janne Lempe for organization of sample sequencing at the Max Planck Institute for Plant Breeding Research. Research was supported by the Deutsche Forschungsgemeinschaft (grants ZA259/7,8; SFB 944 to SZ) and the CAPES-Humboldt Fellowship (grant 99999.007611/2015-03 to MAT).

Author contributions

SZ, AM and MT designed the research. AB, MD, MAT, SK, ES and CK performed the research. All authors analyzed and interpreted the data. AB, MD and SZ wrote the manuscript with support of all authors. AB and MD contributed equally to this work.

ORCID

Marilia Almeida-Trapp https://orcid.org/0000-0002-9980-322X
Axel Mithöfer https://orcid.org/0000-0001-5229-6913
Sabine Zachgo https://orcid.org/0000-0002-6666-1499

References

Albert NW, Thrimawithana AH, McGhie TK, Clayton WA, Deroles SC, Schwinn KE, Bowman JL, Jordan BR, Davies KM. 2018. Genetic analysis of the liverwort *Marchantia polymorpha* reveals that R2R3MYB activation of flavonoid production in response to abiotic stress is an ancient character in land plants. *New Phytologist* **218**: 554–566.

Althoff F, Kopischke S, Zobell O, Ide K, Ishizaki K, Kohchi T, Zachgo S. 2014. Comparison of the *MpEF1α* and *CaMV35* promoters for application in *Marchantia polymorpha* overexpression studies. *Transgenic Research* **23**: 235–244.

Alvarez JP, Furumizu C, Efroni I, Eshed Y, Bowman JL. 2016. Active suppression of a leaf meristem orchestrates determinate leaf growth. *eLife* **5**: e15023.

Araji S, Grammer TA, Gertzen R, Anderson SD, Mikulic-Petkovsek M, Veberic R, Phu ML, Solar A, Leslie CA, Dandekar AM *et al.* 2014. Novel roles for the polyphenol oxidase enzyme in secondary metabolism and the regulation of cell death in walnut. *Plant Physiology* **164**: 1191–1203.

Asakawa Y, Ludwiczuk A, Nagashima F. 2013. Phytochemical and biological studies of bryophytes. *Phytochemistry* **91**: 52–80.

Bell AA. 1981. Biochemical mechanisms of disease resistance. *Annual Review of Plant Physiology and Plant Molecular Biology* **32**: 21–81.

Bienert GP, Chaumont F. 2014. Aquaporin-facilitated transmembrane diffusion of hydrogen peroxide. *Biochimica et Biophysica Acta–General Subjects* **1840**: 1596–1604.

Bindoli A, Rigobello MP, Deeble DJ. 1992. Biochemical and toxicological properties of the oxidation products of catecholamines. *Free Radical Biology and Medicine* **13**: 391–405.

Bowman JL, Kohchi T, Yamato KT, Jenkins J, Shu SQ, Ishizaki K, Yamaoka S, Nishihama R, Nakamura Y, Berger F *et al.* 2017. Insights into land plant evolution garnered from the *Marchantia polymorpha* genome. *Cell* **171**: 287–304.

Busch A, Horn S, Zachgo S. 2014. Differential transcriptome analysis reveals insight into monosymmetric corolla development of the crucifer *Iberis amara*. *BMC Plant Biology* **14**: e285.

Busch A, Zachgo S. 2007. Control of corolla monosymmetry in the Brassicaceae *Iberis amara*. *Proceedings of the National Academy of Sciences, USA* **104**: 16714–16719.

Constabel CP, Ryan CA. 1998. A survey of wound- and methyl jasmonate-induced leaf polyphenol oxidase in crop plants. *Phytochemistry* **47**: 507–511.

Crawford BCW, Nath U, Carpenter R, Coen ES. 2004. *CINCINNATA* controls both cell differentiation and growth in petal lobes and leaves of antirrhinum. *Plant Physiology* **135**: 244–253.

Cui Y, Hu YH, Yu F, Zheng J, Chen LS, Chen QX, Wang Q. 2017. Inhibition kinetics and molecular simulation of *p*-substituted cinnamic acid derivatives on tyrosinase. *International Journal of Biological Macromolecules* **95**: 1289–1297.

Dagnino-Subiabre A, Cassels BK, Baez S, Johansson AS, Mannervik B, Segura-Aguilar J. 2000. Glutathione transferase M2-2 catalyzes conjugation of dopamine and dopa *o*-quinones. *Biochemical and Biophysical Research Communications* **274**: 32–36.

Danisman S, van Dijk ADJ, Bimbo A, van der Wal F, Hennig L, de Folter S, Angenent GC, Immink RGH. 2013. Analysis of functional redundancies within the *Arabidopsis* TCP transcription factor family. *Journal of Experimental Botany* **64**: 5673–5685.

Dietz KJ. 2014. Redox regulation of transcription factors in plant stress acclimation and development. *Antioxidants & Redox Signaling* **21**: 1356–1372.

Dixon P, Edwards R. 2010. Glutathione transferases. *Arabidopsis Book* **8**: e0131.

Doebley J, Stec A, Hubbard L. 1997. The evolution of apical dominance in maize. *Nature* **386**: 485–488.

Dynowski M, Schaaf G, Loque D, Moran O, Ludewig U. 2008. Plant plasma membrane water channels conduct the signalling molecule H_2O_2. *Biochemical Journal* **414**: 53–61.

Efroni I, Blum E, Goldshmidt A, Eshed Y. 2008. A protracted and dynamic maturation schedule underlies *Arabidopsis* leaf development. *Plant Cell* **20**: 2293–2306.

Francoz E, Ranocha P, Nguyen-Kim H, Jamet E, Burlat V, Dunand C. 2015. Roles of cell wall peroxidases in plant development. *Phytochemistry* **112**: 15–21.

Furuya T, Hattori K, Kimori Y, Ishida S, Nishihama R, Kohchi T, Tsukaya H. 2018. ANGUSTIFOLIA contributes to the regulation of three-dimensional morphogenesis in the liverwort *Marchantia polymorpha*. *Development* **145**: dev161398.

Guan PZ, Ripoll JJ, Wang RH, Vuong L, Bailey-Steinitz LJ, Ye DN, Crawford NM. 2017. Interacting TCP and NLP transcription factors control plant responses to nitrate availability. *Proceedings of the National Academy of Sciences, USA* **114**: 2419–2424.

Gutsche N, Holtmannspötter M, Maß L, O'Donoghue M, Busch A, Lauri A, Schubert V, Zachgo S. 2017. Conserved redox-dependent DNA binding of ROXY glutaredoxins with TGA transcription factors. *Plant Direct* **1**: e00030.

Havir E. 1992. The *in vivo* and *in vitro* inhibition of catalase from leaves of *Nicotiana sylvestris* by 3-amino-1,2,4-triazole. *Plant Physiology* **99**: 533–537.

He H, Van Breusegem F, Mhamdi A. 2018. Redox-dependent control of nuclear transcription in plants. *Journal of Experimental Botany* **69**: 3359–3372.

Herve C, Dabos P, Bardet C, Jauneau A, Auriac MC, Ramboer A, Lacout F, Tremousaygue D. 2009. *In vivo* interference with AtTCP20 function induces severe plant growth alterations and deregulates the expression of many genes important for development. *Plant Physiology* **149**: 1462–1477.

Hideg E, Jansen MAK, Strid A. 2013. UV-B exposure, ROS, and stress: inseparable companions or loosely linked associates? *Trends in Plant Science* **18**: 107–115.

Hooijmaijers C, Rhee JY, Kwak KJ, Chung GC, Horie T, Katsuhara M, Kang H. 2012. Hydrogen peroxide permeability of plasma membrane aquaporins of *Arabidopsis thaliana*. *Journal of Plant Research* **125**: 147–153.

Jansen MAK, Gaba V, Greenberg BM. 1998. Higher plants and UV-B radiation: balancing damage, repair and acclimation. *Trends in Plant Science* **3**: 131–135.

Junglee S, Urban L, Sallanon H, Lopez-Lauri F. 2014. Optimized assay for hydrogen peroxide determination in plant tissue using potassium iodide. *American Journal of Analytical Chemistry* **5**: 730–736.

Kieffer M, Master V, Waites R, Davies B. 2011. TCP14 and TCP15 affect internode length and leaf shape in Arabidopsis. *The Plant Journal* **68**: 147–158.

Komarov DA, Slepneva IA, Glupov VV, Khramtsov VV. 2005. Superoxide and hydrogen peroxide formation during enzymatic oxidation of DOPA by phenoloxidase. *Free Radical Research* **39**: 853–858.

Kopischke S, Schussler E, Althoff F, Zachgo S. 2017. TALEN-mediated genome-editing approaches in the liverwort *Marchantia polymorpha* yield high efficiencies for targeted mutagenesis. *Plant Methods* **13**: e20.

Kosugi S, Ohashi Y. 1997. PCF1 and PCF2 specifically bind to *cis* elements in the rice proliferating cell nuclear antigen gene. *Plant Cell* **9**: 1607–1619.

Kosugi S, Ohashi Y. 2002. DNA binding and dimerization specificity and potential targets for the TCP protein family. *The Plant Journal* **30**: 337–348.

Kunz S, Burkhardt G, Becker H. 1994. Riccionidins A and B, anthocyanidins from the cell walls of the liverwort *Ricciocarpos natans*. *Phytochemistry* **35**: 233–235.

Li JLY, Sulaiman M, Beckett RP, Minibayeva FV. 2010. Cell wall peroxidases in the liverwort *Dumortiera hirsuta* are responsible for extracellular superoxide production, and can display tyrosinase activity. *Physiologia Plantarum* **138**: 474–484.

Li L, Steffens JC. 2002. Overexpression of polyphenol oxidase in transgenic tomato plants results in enhanced bacterial disease resistance. *Planta* **215**: 239–247.

Li NH, Zhao M, Liu TF, Dong LD, Cheng Q, Wu JJ, Wang L, Chen X, Zhang CZ, Lu WC *et al.* 2017. A novel soybean dirigent gene *GmDIR22* contributes to promotion of lignan biosynthesis and enhances resistance to *Phytophthora sojae*. *Frontiers in Plant Science* **8**: e1185.

Li ST, Zachgo S. 2013. TCP3 interacts with R2R3-MYB proteins, promotes flavonoid biosynthesis and negatively regulates the auxin response in *Arabidopsis thaliana*. *The Plant Journal* **76**: 901–913.

Lin WL, Peng YH, Li GW, Arora R, Tang ZC, Su WA, Cai WM. 2007. Isolation and functional characterization of PgTIP1, a hormone-autotrophic cells-specific tonoplast aquaporin in ginseng. *Journal of Experimental Botany* **58**: 947–956.

Lu D, Wang T, Persson S, Mueller-Roeber B, Schippers JHM. 2014. Transcriptional control of ROS homeostasis by KUODA1 regulates cell expansion during leaf development. *Nature Communications* **5**: e3767.

Luo D, Carpenter R, Vincent C, Copsey L, Coen E. 1996. Origin of floral asymmetry in *Antirrhinum*. *Nature* **383**: 794–799.

Maberly SC. 2014. The fitness of the environments of air and water for photosynthesis, growth, reproduction and dispersal of photoautotrophs: an evolutionary and biogeochemical perspective. *Aquatic Botany* **118**: 4–13.

Martin-Trillo M, Cubas P. 2010. TCP genes: a family snapshot ten years later. *Trends in Plant Science* **15**: 31–39.

Maurel C, Boursiac Y, Luu DT, Santoni V, Shahzad Z, Verdoucq L. 2015. Aquaporins in plants. *Physiological Reviews* **95**: 1321–1358.

Mhamdi A, Queval G, Chaouch S, Vanderauwera S, Van Breusegem F, Noctor G. 2010. Catalase function in plants: a focus on *Arabidopsis* mutants as stress-mimic models. *Journal of Experimental Botany* **61**: 4197–4220.

Mhamdi A, Van Breusegem F. 2018. Reactive oxygen species in plant development. *Development* **145**: dev164376.

Mittler R. 2017. ROS are good. *Trends in Plant Science* **22**: 11–19.

Morris JL, Puttick MN, Clark JW, Edwards D, Kenrick P, Pressel S, Wellman CH, Yang ZH, Schneider H, Donoghue PCJ. 2018. The timescale of early land plant evolution. *Proceedings of the National Academy of Sciences, USA* **115**: E2274–E2283.

Munoz P, Huenchuguala S, Paris I, Segura-Aguilar J. 2012. Dopamine oxidation and autophagy. *Parkinson's Disease* **2012**: 920953.

Nath U, Crawford BCW, Carpenter R, Coen E. 2003. Genetic control of surface curvature. *Science* **299**: 1404–1407.

Navaud O, Dabos P, Carnus E, Tremousaygue D, Herve C. 2007. TCP transcription factors predate the emergence of land plants. *Journal of Molecular Evolution* **65**: 23–33.

Nishiyama T, Sakayama H, de Vries J, Buschmann H, Saint-Marcoux D, Ullrich KK, Haas FB, Vanderstraeten L, Becker D, Lang D *et al.* 2018. The *Chara* genome: secondary complexity and implications for plant terrestrialization. *Cell* **174**: 448–464.

Noctor G, Reichheld JP, Foyer CH. 2018. ROS-related redox regulation and signaling in plants. *Seminars in Cell & Developmental Biology* **80**: 3–12.

Palatnik JF, Allen E, Wu XL, Schommer C, Schwab R, Carrington JC, Weigel D. 2003. Control of leaf morphogenesis by microRNAs. *Nature* **425**: 257–263.

Paniagua C, Bilkova A, Jackson P, Dabravolski S, Riber W, Didi V, Houser J, Gigli-Bisceglia N, Wimmerova M, Budinska E *et al.* 2017. Dirigent proteins in plants: modulating cell wall metabolism during abiotic and biotic stress exposure. *Journal of Experimental Botany* **68**: 3287–3301.

Peters K, Gorzolka K, Bruelheide H, Neumann S. 2018. Seasonal variation of secondary metabolites in nine different bryophytes. *Ecology and Evolution* **8**: 9105–9117.

Queval G, Issakidis-Bourguet E, Hoeberichts FA, Vandorpe M, Gakiere B, Vanacker H, Miginiac-Maslow M, Van Breusegem F, Noctor G. 2007. Conditional oxidative stress responses in the Arabidopsis photorespiratory mutant *cat2* demonstrate that redox state is a key modulator of daylength-dependent gene expression, and define photoperiod as a crucial factor in the regulation of H_2O_2-induced cell death. *The Plant Journal* **52**: 640–657.

Remiao F, Milhazes N, Borges F, Carvalho F, Bastos ML, Lemos-Amado F, Domingues P, Ferrer-Correia A. 2003. Synthesis and analysis of aminochromes by HPLC-photodiode array. Adrenochrome evaluation in rat blood. *Biomedical Chromatography* **17**: 6–13.

Schippers JHM, Foyer CH, van Dongen JT. 2016. Redox regulation in shoot growth, SAM maintenance and flowering. *Current Opinion in Plant Biology* **29**: 121–128.

Shigeto J, Tsutsumi Y. 2016. Diverse functions and reactions of class III peroxidases. *New Phytologist* **209**: 1395–1402.

Shimamura M. 2016. *Marchantia polymorpha*: taxonomy, phylogeny and morphology of a model system. *Plant and Cell Physiology* **57**: 230–256.

Smirnoff N, Arnaud D. 2019. Hydrogen peroxide metabolism and functions in plants. *New Phytologist* **221**: 1197–1214.

Solano F. 2014. Melanins: skin pigments and much more – types, structural models, biological functions, and formation routes. *New Journal of Science* **2014**: e498276.

Sugano SS, Nishihama R, Shirakawa M, Takagi J, Matsuda Y, Ishida S, Shimada T, Hara-Nishimura I, Osakabe K, Kohchi T. 2018. Efficient CRISPR/Cas9-based genome editing and its application to conditional genetic analysis in *Marchantia polymorpha*. *PLoS ONE* **13**: e0205117.

Sugumaran M. 2016. Reactivities of quinone methides versus *o*-quinones in catecholamine metabolism and eumelanin biosynthesis. *International Journal of Molecular Sciences* **17**: E1576.

Tavladoraki P, Cona A, Angelini R. 2016. Copper-containing amine oxidases and FAD-dependent polyamine oxidases are key players in plant tissue differentiation and organ development. *Frontiers in Plant Science* **7**: e824.

Terui K. 1975. Abnormalities in *Marchantia polymorpha* L. *Annual Report of the Faculty of Education, University of Iwate* **35**: 61–67.

Thipyapong P, Hunt MD, Steffens JC. 2004. Antisense downregulation of polyphenol oxidase results in enhanced disease susceptibility. *Planta* **220**: 105–117.

Tian YC, Fan M, Qin ZX, Lv HJ, Wang MM, Zhang Z, Zhou WY, Zhao N, Li XH, Han C *et al.* 2018. Hydrogen peroxide positively regulates brassinosteroid signaling through oxidation of the BRASSINAZOLE-RESISTANT1 transcription factor. *Nature Communications* **9**: e1063.

Tian T, Liu Y, Yan HY, You Q, Yi X, Du Z, Xu WY, Su Z. 2017. AGRIGO v2.0: a GO analysis toolkit for the agricultural community, 2017 update. *Nucleic Acids Research* **45**: W122–W129.

Tian S, Wang XB, Li P, Wang H, Ji HT, Xie JY, Qiu QL, Shen D, Dong HS. 2016. Plant aquaporin AtPIP1;4 links apoplastic H_2O_2 induction to disease immunity pathways. *Plant Physiology* **171**: 1635–1650.

Tsukagoshi H. 2016. Control of root growth and development by reactive oxygen species. *Current Opinion in Plant Biology* **29**: 57–63.

Tsukagoshi H, Busch W, Benfey PN. 2010. Transcriptional regulation of ROS controls transition from proliferation to differentiation in the root. *Cell* **143**: 606–616.

Viola IL, Camoirano A, Gonzalez DH. 2016. Redox-dependent modulation of anthocyanin biosynthesis by the TCP transcription factor TCP15 during exposure to high light intensity conditions in Arabidopsis. *Plant Physiology* **170**: 74–85.

Viola IL, Guttlein LN, Gonzalez DH. 2013. Redox modulation of plant developmental regulators from the class I TCP transcription factor family. *Plant Physiology* **162**: 1434–1447.

Vogt T. 2010. Phenylpropanoid biosynthesis. *Molecular Plant* **3**: 2–20.

de Vries J, Archibald JM. 2018. Plant evolution: landmarks on the path to terrestrial life. *New Phytologist* **217**: 1428–1434.

de Vries J, de Vries S, Slamovits CH, Rose LE, Archibald JM. 2017. How embryophytic is the biosynthesis of phenylpropanoids and their derivatives in streptophyte algae? *Plant and Cell Physiology* **58**: 934–945.

Wang XY, Gao J, Zhu Z, Dong XX, Lei Wang X, Ren GD, Zhou X, Kuai BK. 2015. TCP transcription factors are critical for the coordinated regulation of *ISOCHORISMATE SYNTHASE 1* expression in *Arabidopsis thaliana*. *The Plant Journal* **82**: 151–162.

Waszczak C, Carmody M, Kangasjärvi J. 2018. Reactive oxygen species in plant signaling. *Annual Review of Plant Biology* **69**: 209–236.

Yin R, Messner B, Faus-Kessler T, Hoffmann T, Schwab W, Hajirezaei MR, von Saint Paul V, Heller W, Schaffner AR. 2012. Feedback inhibition of the general phenylpropanoid and flavonol biosynthetic pathways upon a compromised flavonol-3-*O*-glycosylation. *Journal of Experimental Botany* **63**: 2465–2478.

Zeng J, Dong ZC, Wu HJ, Tian ZX, Zhao Z. 2017. Redox regulation of plant stem cell fate. *Embo Journal* **36**: 2844–2855.

Supporting Information

Additional Supporting Information may be found online in the Supporting Information section at the end of the article.

Fig. S1 Genome-editing of the Mp*TCP1* locus to generate Mp*TCP1* knockout mutants in *Marchantia polymorpha*.

Fig. S2 UV chromatogram and MS analyses for riccionidin detection in Marchantia.

Fig. S3 SDS gel and Western blot.

Fig. S4 Gametangiophore phenotypes of male and female *Marchantia polymorpha* Mp*tcp1*^{ge} lines.

Fig. S5 Comparison of Mp*TCP1* expression in vegetative and sexual Marchantia tissues.

Fig. S6 Effect of 3-AT on gemmae growth.

Fig. S7 Loss of Mp*TCP1* function does not result in pigment synthesis and H_2O_2 accumulation in Mp*tcp1*^{ge} archegoniophores.

Methods S1 Additional methodological details are given for data presented in Figs S1 - S7.

Table S1 List of all primer sequences used in the study.

Table S2 Quantification of reduced thallus growth observed in Mp*tcp1*^{ge} lines.

Table S3 List of accession numbers from gene groups involved in ROS metabolism or pigment synthesis from all differentially expressed genes responding to loss of Mp*TCP1* function.

Table S4 Quantification of reduced thallus growth of Marchantia wild-type gemmae grown on 3-AT.

Table S5 Metabolome analysis of Mp*tcp1*^{ge} lines.

Please note: Wiley Blackwell are not responsible for the content or functionality of any Supporting Information supplied by the authors. Any queries (other than missing material) should be directed to the *New Phytologist* Central Office.